

Sensitive Detection of Nuclear Quadrupole Interactions in Solids*

R. E. SLUSHER†

University of California, Berkeley, California and Bell Telephone Laboratories, Murray Hill, New Jersey‡

AND

E. L. HAHN

University of California, Berkeley, California

(Received 28 August 1967)

The pure nuclear quadrupole resonance of a low-abundance spin species in zero field is observed for molar concentrations as low as one part in 10^7 by the application of a nuclear-double-resonance method. The quadrupole resonance is measured in terms of a decrease in the magnetic order of abundant nuclei which are dipolar-coupled to the low-abundance nuclear species. The double-resonance process is analyzed from the point of view of two energy reservoirs coupled by a dipolar perturbation, and spin diffusion among abundant nuclei is included phenomenologically. Radio-frequency power, which causes the main quadrupole transitions of rare spins, is frequency-modulated to provide saturation in the rotating frame and to enable identification of unknown spin transitions. The pure nuclear quadrupole resonance of Na and Cl nuclei near impurities and imperfections in NaCl is measured. Particular attention is given to the resonances associated with K^+ and Br^- ions injected as impurities into the NaCl lattice. An unsuccessful search in zero field has been made for the naturally abundant 0.0156% deuterium quadrupole resonance in $CaSO_4 \cdot 2H_2O$ and $C_{10}H_8$, where the proton resonance is monitored as the abundant nuclear species. The proton dipolar absorption in zero magnetic field is anomalously broad and overlaps too much with the deuterium quadrupole resonance to permit independent observation of the latter. A narrowing of proton dipolar absorption in zero field is observed for strong radio-frequency fields larger than internal dipole fields.

I. INTRODUCTION

NUCLEAR-DOUBLE-RESONANCE techniques¹⁻⁶ have been applied to detect Zeeman and electric quadrupole-resonance transitions of nuclei at very low radio frequencies or at very low concentrations in solids. Further developments of an ultrasensitive method² for detecting pure nuclear quadrupole interactions are described in this paper. The spectroscopy is carried out by observations of strong nuclear-resonance signals from an abundant nuclear spin species prepared in an ordered metastable magnetic state. This state is often referred to as existing in a rotating frame of reference, which implies that the abundant nuclei are ordered or aligned with respect to rotating radio-frequency fields, or with respect to internal dipolar fields. The literal concept of a rotating frame, however, is not always possible, and the ordered state is more generally conceived as a transformed one in a new interaction representation. The entire spin ensemble is characterized as metastable because it is

no longer in thermal equilibrium with the lattice. After its preparation the spin order normally dies away in a spin-lattice relaxation time, which is chosen to be long. If a second radio-frequency field is applied to the sample during this metastable condition, it is possible to excite the spin resonance of a foreign spin species (B spins), which is dipolar-coupled to the observed species (A spins), and therefore induce an additional loss of order among the A spins. The apparent relaxation loss rate of the order in the A spins can then be increased from the natural spin-lattice relaxation rate T_{1A}^{-1} to a rate $T_{1A}^{-1} + R_{AB}$, where R_{AB} is the transfer rate of spin ordering from the A to the B system. For long relaxation times T_{1A} , of about 1 min, concentrations of B nuclei estimated to be as low as 10^{-7} moles per mole of A nuclei can be detected. In order to achieve this sensitivity, the spin order, which is transferred from the A system to the B system, must be continually destroyed by saturation of the magnetization which builds up along the effective field applied to the B spins in the rotating frame. Otherwise, the order in both A and B systems reaches a dynamic equilibrium or a "common spin temperature," and further reduction of the order in the A system ceases. A novel scheme for achieving this saturation in the rotating frame (rotary saturation) is introduced in this investigation by modulating the frequency of the main rf excitation which is at resonance with the B spins transition. It is also shown that the modulation method allows a direct identification of the particular B -spin-species which is associated with a given nuclear-quadrupole transition.

Nuclear-quadrupole interactions in NaCl are studied here as a good example of information to be gained

* Work supported by the National Science Foundation and the U.S. Office of Naval Research.

† Major portion based on a thesis submitted by this author in partial fulfillment of the requirements for the Ph.D. degree at the University of California, Berkeley, Calif.

‡ Present address.

¹ A. G. Redfield, Phys. Rev. **130**, 589 (1963).

² R. E. Slusher and E. L. Hahn, Phys. Rev. Letters **12**, 246 (1964).

³ S. Hartmann and E. L. Hahn, Phys. Rev. **128**, 2024 (1962).

⁴ F. M. Lurie and C. P. Slichter, Phys. Rev. Letters **10**, 403 (1963).

⁵ D. McArthur, R. E. Walstedt, and E. L. Hahn, Phys. Letters **15**, 7 (1965).

⁶ D. McArthur, R. E. Walstedt, and E. L. Hahn (to be published); E. L. Hahn, in *Proceedings of the Fourteenth Colloque Ampère Conference, Ljubljana, Yugoslavia* (North-Holland Publishing Co., Amsterdam, to be published).

by the double resonance method. Pure NaCl is a cubic salt; the Na and Cl nuclear-quadrupole moments, each with spin $I = \frac{3}{2}$, are at sites of zero electric field gradient, unless they happen to be near impurities or lattice imperfections where the cubic symmetry is destroyed. For example, a K^+ ion which substitutes for a Na^+ ion will cause displacement of neighboring ions, and will induce characteristic electric dipoles and electric field gradients in its immediate neighborhood. The Na and Cl pure nuclear-quadrupole-resonance transitions (NQR) expected near such impurities may range from 10 kc/sec to about 5 mc/sec. It is the NQR of these Na or Cl nuclei in noncubic sites which are dealt with here, and not with the NQR of the substitutional impurities themselves. It is possible however, for substitutional ions to be quadrupole-coupled if they are located at sites where the electric field gradient is finite. The double-resonance method can be applied as well to investigate the NQR of rare isotopes such as D, O^{17} , S^{33} , Ca^{43} , etc., in suitable crystals which can provide a strong resonance from an abundant nuclear species. In zero magnetic field, amorphous solids and crystalline powders can be studied because the NQR transition is uniquely determined by internal electric fields and is not smeared out completely by magnetic field broadening. In a high magnetic field the NQR splitting which accompanies the Zeeman transitions can only be measured with precision in single crystals. In this case the double-resonance technique⁶ can also be applied, but it is modified from the experimental procedure emphasized in this paper, and will not be discussed here.

Figure 1 shows the time sequence for detecting a B -spin zero-field quadrupole resonance. First the A nuclei are polarized in high magnetic field ($H_0 \cong 10$ kG) for a high-field spin-lattice relaxation time T_1 . In NaCl the abundant A nuclei will actually consist of both Cl and Na nuclei in cubic sites, although the Na nuclear resonance signal will be the only nuclear species observed directly. The B resonance of rare Na and Cl nuclei is excited at noncubic sites near impurities after the sample is removed from the magnet to a region of zero external field for a time period $t \cong \tau_0$.

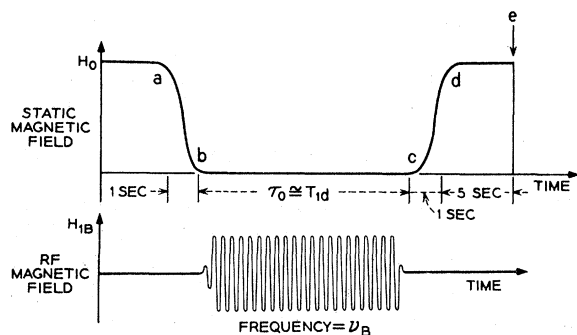


FIG. 1. Low-field double-resonance sequence. The rf field H_{1B} is usually phase- or frequency-modulated.

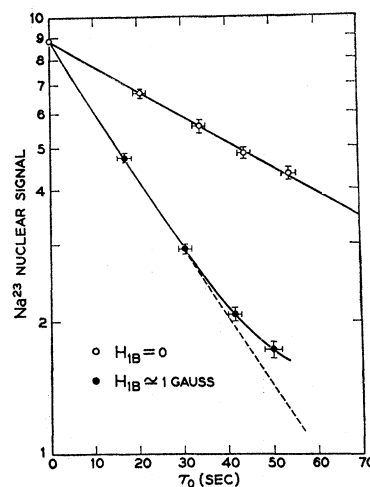


FIG. 2. Decay of Na^{23} magnetization after $t = \tau_0$ sec in zero static magnetic field. For $H_{1B} = 0$, the upper slope is a measure of T_{1d} , the zero-field spin-lattice relaxation. The lower curve is for ν_B of 280.5 kc/sec. The B nuclei responsible for the added double-resonance relaxation rate were identified as Cl^{35} nuclei near K^+ substitutional impurities. The sample was a powder with K^+ molar concentration of 0.1%. Nonexponential behavior may be caused by inhomogeneous H_{1B} .

In general, the sample demagnetization is performed adiabatically in a time short compared to the spin-lattice relaxation time [(a) to (b) in Fig. 1]. In the demagnetized state the entropy of the A system is formally preserved. However, the order it represents in terms of alignment of nuclei along local dipole fields will decay in a modified spin-lattice time constant T_{1d} , which is generally shorter than the high field T_1 . The B nuclei are irradiated with an rf field intensity H_{1B} at the time points (b) to (c), lasting for a time τ_0 of the order of T_{1d} , indicated in Fig. 1. The double-resonance cross-relaxation rate R_{AB} is then greatest when

$$\gamma_B H_{1B} \cong \gamma_A h_L \quad (1)$$

and

$$\nu_B = \nu_Q,$$

where h_L is the mean local dipole field at the sites of A nuclei, γ is the gyromagnetic ratio, and ν_Q is the quadrupole resonance frequency of the B nuclei. At point (c) the sample is adiabatically remagnetized by the former polarizing field. Any remaining order of the A nuclei is measured by applying a 90° pulse at time point (e), and the intensity of the free nuclear-induction decay is recorded. The sequence of Fig. 1 is repeated following each remagnetization. As each sequence is repeated, the frequency ν_B applied to the B system in search of NQR transitions is adjusted to a new value, increasing by 1 kc for each successive sequence. A decrease in magnetization at point (e) signifies the onset of a spin resonance. Figure 2 shows a plot of the free-induction amplitude of the Na resonance in NaCl as a function of time τ_0 in zero field for fixed irradiation

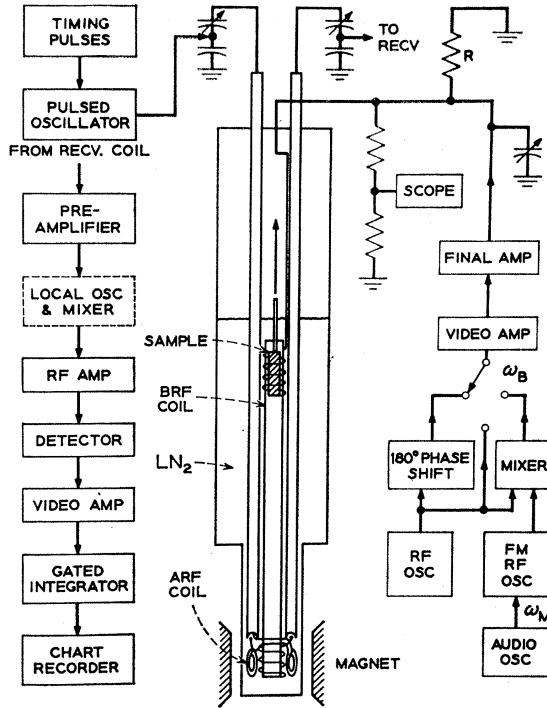


FIG. 3. Low-field double-resonance apparatus. Sample is shown in low-field position where H_{1B} is applied. Right side shows apparatus for producing H_{1B} , left side shows apparatus for measuring A -spin magnetization in high magnetic field.

frequency ν_B . Figure 3 gives a block diagram of the experimental apparatus.

II. ZERO-FIELD NUCLEAR-DOUBLE-RESONANCE THEORY

A. Nuclear-Quadrupole Interaction Representation

The Hamiltonian of interest for the nuclear-quadrupole double-resonance process in zero field is

$$H = H_{QB} + H_{AA} + H_{rf B} + H_{AB}, \quad (2)$$

where the magnetic dipole interaction between A and B nuclei is

$$H_{AB} = \sum_{j < k}^{A, B} h_{ABjk},$$

$$h_{AB} = \sum_{M=-2}^{+2} h_{AB}^M,$$

$$h_{AB}^0 = B[I_z S_z - (\mathbf{I} \cdot \mathbf{S})/3],$$

$$h_{AB}^1 = C(I_z S_+ + I_+ S_z),$$

$$h_{AB}^2 = E(I_+ S_+),$$

$$B = \frac{1}{2}(3\hbar^2 \gamma_A \gamma_B) [(1 - 3 \cos^2 \theta)/r^3],$$

$$C = \frac{1}{2}(3\hbar^2 \gamma_A \gamma_B) [(\sin \theta \cos \theta)/r^3] \exp(-i\phi),$$

$$E = \frac{1}{4}(3\hbar^2 \gamma_A \gamma_B) [(\sin^2 \theta)/r^3] \exp(-2i\phi). \quad (3)$$

The internuclear distance \mathbf{r} makes an angle θ with the chosen z axis, ϕ is the azimuthal angle, and

$$h_{AB}^{-M} = (h_{AB}^M)^\dagger.$$

Dipolar interactions among A nuclei are represented by H_{AA} , where H_{AA} has the same form as H_{AB} (I is used to denote A nuclear-spin operators, S for B nuclear-spin operators). The rf B interaction is represented by $H_{rf B}$. The B nuclei are assumed to be rare and spatially distributed so that mutual dipolar interactions among them may be neglected. The interaction of the B -spin electric-quadrupole moments with electric field gradients in the solid is given by

$$H_{QB} = \sum_j^B h_{QBj}, \quad (4)$$

where the single spin operator is

$$h_{QB} = K[3S_z^2 - S(S+1) + \frac{1}{2}\eta(S_+^2 + S_-^2)], \quad (5)$$

and

$$K = e^2 q Q / 4S(2S-1). \quad (6)$$

The electric field gradient is

$$eq_{zz} = V_{zz} \quad (7)$$

in the principal axis frame, where the field-gradient tensor is diagonal, and we choose

$$|V_{zz}| \geq |V_{xx}| \geq |V_{yy}|, \quad (8)$$

so that the asymmetry parameter is

$$\eta = [|V_{xx}| - |V_{yy}|] / |V_{zz}|, \quad (9)$$

where

$$1 \geq \eta \geq 0.$$

Only the B nuclei are assumed to interact appreciably with the linearly polarized applied rf field. Therefore

$$H_{rf B} = -2\hbar\gamma_B \cos\omega_B t \sum_{j, \mu} H_{1B\mu} S_{\mu j}, \quad (10)$$

where the μ index pertains to x , y , or z directions. For the B spins we will assume an axially symmetric electric field gradient with $\eta=0$ and $S=\frac{3}{2}$. Therefore, only the x and y components of Eq. (10) will effect transitions between the two quadrupole energy levels $|m_z\rangle = |\pm\frac{3}{2}\rangle$ and $|m_z\rangle = |\pm\frac{1}{2}\rangle$. The resonance condition for transitions between these levels is given by

$$\omega_B = \omega_Q = e^2 q Q / 2\hbar = 6K/\hbar. \quad (11)$$

The A and B spin-lattice relaxation interactions are assumed to be very weak and independent of the interactions represented by H_{AA} , $H_{rf B}$, and H_{AB} . The A reservoir of spins can be directly assigned a spin temperature T_A in the laboratory frame if the nuclei are at equilibrium among themselves. For T_A independent of lattice coordinate \mathbf{r} , the density matrix of the

A system is

$$\rho_A = \frac{\exp[-(H_{AA}/kT_A)]}{\text{Tr}[\exp(-H_{AA}/kT_A)]}, \quad (12)$$

where it is assumed that the energy in the interaction H_{AB} is negligible compared to the H_{AA} interaction. During the polarization process in high field H_0 (see Fig. 1) the spin temperature $T_A(H_0)$ approaches the lattice temperature T_L . After adiabatic demagnetization the spin temperature becomes

$$T_A(0) \cong (h_L/H_0) T_L, \quad (13)$$

where

$$h_L^2 = \text{Tr}\{H_{AA}^2\}/\text{Tr}\{M_z^2\}, \quad (14)$$

and $M_z = \hbar \sum_j \gamma_j I_{z_j}$ is a sum over all the nuclei which contribute to h_L , the mean local field established by the A -spin reservoir. Without double-resonance cross relaxation, the spin temperature of the A spins increases as

$$T_A(t) \cong T_A(0) \exp\{t/T_{1d}\}, \quad (15)$$

where it is assumed that $T_A(t) \ll T_L$, and T_{1d} is the spin-lattice relaxation time in zero external field. For $H_0 \cong 10$ kG the ratio $T_1(H_0)/T_{1d}$ ranges from 2 to 10^6 , depending upon the type of lattice coupling and the lattice temperature. In the presence of the double-resonance interaction, Eq. (15) becomes

$$T_A(t) = T_A(0) \exp\{t[(1/T_{1d}) + (1/\tau_{AB})]\}, \quad (16)$$

where

$$R_{AB} = \tau_{AB}^{-1}.$$

In order to evaluate τ_{AB} the state of the B nuclei must now be described. Spin temperature cannot be ascribed to the B nuclei in the laboratory frame because $H_{rf B}$ is time-dependent, and no time-independent equilibrium state can be defined for the B spins in the laboratory frame of reference. Therefore, we use the unitary transformation

$$U_Q = \exp\left\{-\frac{1}{\hbar} (i\omega_B t) \sum_j [3S_{z_j}^2 - \mathbf{S}_j^2]\right\} \quad (17)$$

to obtain an interaction representation where the Hamiltonian Eq. (2) with $\eta=0$ becomes time-independent; namely,

$$\begin{aligned} H^* &= U_Q H U_Q^{-1} - (\hbar\omega_B/6K) H_{QB} \\ &= [1 - (\hbar\omega_B/6K)] H_{QB} + H_{AA} + H_{AB}^{*'} + H_{rf B}^{*'} \end{aligned} \quad (18)$$

Primed terms indicate that components of H^* oscillating at ω and 2ω are dropped since they average to zero.

The transformation which conveniently expresses U_Q in Eq. (17) has been demonstrated previously.⁷

⁷ G. W. Leppelmeier and E. L. Hahn, Phys. Rev. **142**, 179 (1966); see also M. Goldman and A. Landesman, *ibid.* **132**, 610 (1963).

The matrix for U_Q can be expressed in terms of subsets of Pauli spin matrices. For spin $S = \frac{3}{2}$ the 4×4 matrix representation for single-spin operators can be decomposed into four 2×2 matrices. These submatrices can be then written as linear combinations of Pauli spin matrices. Using this notation we obtain

$$U_Q = \exp\left[-\frac{1}{2} (i\omega t) \sum_j (\sigma_{azj} - \sigma_{bzj})\right] \quad (19)$$

and

$$H_{rf B}^{*'} = \hbar\omega_{1B} \frac{1}{2} \sqrt{3} \sum_j (\sigma_{azj} + \sigma_{bzj}), \quad (20)$$

where σ_{ax} is the Pauli spin matrix σ_x in the a corner of the 4×4 matrix

$$\begin{array}{c} +\frac{3}{2} \\ +\frac{1}{2} \\ -\frac{1}{2} \\ -\frac{3}{2} \end{array} \left\| \begin{array}{cc} +\frac{3}{2} + \frac{1}{2} & -\frac{1}{2} - \frac{3}{2} \\ a & u \\ \hline l & b \end{array} \right\| \quad (21)$$

Also,

$$H_{AB}^{*'} = \sum_{j,k}^{A,B} h_{ABjk}^{*'}, \quad (22)$$

where, for a given spin pair,

$$\begin{aligned} h_{AB}^{*'} &= \frac{2}{3} B I_z S_z \\ &+ \frac{1}{6} (B\sqrt{3}) [(\mu_{a+}\sigma_{l+} + \mu_{b+}\sigma_{l+} + \sigma_{u-}\mu_{a-} + \sigma_{u-}\mu_{b-}) \\ &+ \mu_{u-}\sigma_{l+} + \sigma_{u-}\mu_{l+}] \\ &+ C(I_z\sigma_{u-} + S_z\mu_{u-}) + C^*(I_z\sigma_{l+} + S_z\mu_{l+}) \\ &+ E[\frac{1}{2}\sqrt{3}(\mu_{a+}\sigma_{u-} + \mu_{b+}\sigma_{u-}) + \mu_{u-}\sigma_{u-}] \\ &+ E^*[\frac{1}{2}\sqrt{3}(\mu_{a-}\sigma_{l+} + \mu_{b-}\sigma_{l+}) + \mu_{l+}\sigma_{l+}], \end{aligned} \quad (23)$$

and C^* and E^* are complex conjugates.

The symbols σ and μ represent Pauli spin matrices for B and A nuclei, respectively, and for the A spin we take $I = \frac{3}{2}$ in anticipation of treating the problem of NQR double resonance in NaCl. In obtaining Eqs. (20) and (21) the exponential operators have been expanded and the direct commutation and multiplication rules are applied. For the applied rf field at the exact B -spin quadrupole resonance expressed by Eq. (11), the effective Hamiltonian in the interaction representation is

$$H^* = H_{AA} + \sum_{j < k}^{A,B} h_{ABjk}^{*'} + \sum_j^B h_{rf B}^{*'} \quad (24)$$

Consider the energy levels for a single B nucleus in this representation. $h_{rf B}^{*'}$ can be diagonalized, and we find the following eigenfunctions and eigenvalues

using the $|m_z\rangle$ states:

Eigenfunctions	Eigenvalues
$\frac{1}{\sqrt{2}}[+\frac{3}{2}\rangle - +\frac{1}{2}\rangle]$	$+\frac{1}{2}\sqrt{3}\hbar\omega_{1B}$,
$\frac{1}{\sqrt{2}}[-\frac{1}{2}\rangle - -\frac{3}{2}\rangle]$	
$\frac{1}{\sqrt{2}}[+\frac{3}{2}\rangle + +\frac{1}{2}\rangle]$	$-\frac{1}{2}\sqrt{3}\hbar\omega_{1B}$.
$\frac{1}{\sqrt{2}}[-\frac{3}{2}\rangle + -\frac{1}{2}\rangle]$	

These levels are broadened by the interaction H_{AB}^{*} . The terms H_{rfB}^{*} and H_{AA} can be thought of as establishing two energy reservoirs coupled by H_{AB}^{*} . H_{rfB}^{*} is time-independent and a spin temperature T_B can be used to describe a Boltzmann occupation of the levels above if the B nuclei are in contact with the A nuclei at a uniform spin temperature T_A . Therefore, we can write the quasiequilibrium density matrix

$$\rho_B^* = [\exp(-H_{rfB}^{*}/kT_B)]/\text{Tr}(1), \quad (25)$$

and the total density matrix in the interaction representation is

$$\rho^* = \rho_A + \rho_B^* \cong 1 - [H_{AA}/kT_A \text{Tr}(1)] - [H_{rfB}^{*}/kT_B \text{Tr}(1)], \quad (26)$$

B. Double-Resonance Dynamics

Using the interaction representation and energy reservoirs described above, a simple phenomenological model will now be shown which describes in second order the dynamics of the double-resonance process for rare spins. It will be assumed that H_{AB}^{*} can be treated as a small interaction compared to the B -spin Zeeman interaction with H_{1B} , and to the intradipolar interactions among the A nuclei. This makes possible the use of perturbation theory which describes the transfer of disorder from the B to the A nuclei by simple rate equations. In reality this perturbation approach does not appear to be strictly valid since the double-resonance condition, Eq. (1), suggests that the intradipolar A -spin interaction is of the order of the perturbation interaction H_{AB}^{*} in our study of NaCl. However, for B nuclei near impurity levels in the NaCl lattice, there exists a series of quadrupole-split Na and Cl nuclei as r increases from the B nuclei to the purely dipolar-coupled A nuclei in cubic sites. These quadrupole interactions restrict dipolar spin flips to nuclei in the states pertaining to the lower spin degenerate ($S = < \frac{1}{2}$) quadrupole levels, and decreases the effective H_{AB}^{*} interaction. The perturbation approach therefore becomes plausible, but only approximate in this case.

The A - and B -spin energy reservoirs are assigned temperatures $T_A(\mathbf{r}, t)$ and $T_B(t)$, respectively. Since the B nuclei may be spaced apart by hundreds of lattice parameters, one must consider the possibility that T_A is a function of position in regions devoid of nuclei because of the finite spin-diffusion rate among A nuclei. B nuclei may be assigned a spin tempera-

ture by virtue of their contact with neighboring A nuclei. Randomly distributed B nuclei in a lattice of A nuclei with position-dependent temperature cannot be assigned a unique spin temperature, but can be considered to have an ensemble averaged temperature $T_B(t)$.

$T_A(\mathbf{r}, t)$ will be assumed to be a function of radius from the B nuclei, and the diffusion among the A spins is therefore assumed to be isotropic. This is only an approximation, since diffusion in a cubic crystal is expected to be faster along $\langle 111 \rangle$ directions than along $\langle 100 \rangle$ directions. A qualitative representation of the model is shown in Fig. 4. B nuclei interact directly with A nuclei out to a radius r_0 , where the A - B dipolar interaction becomes very small compared to the A - A interactions. From r_0 to $\frac{1}{2}r_{BB}$ the spin disorder propagates due to A -spin diffusion, where r_{BB} defines the mean distance between B nuclei. Conservation of energy shared among the A and B reservoirs, assuming negligible spin-lattice relaxation, requires that

$$\partial \bar{\beta}_A(t)/\partial t = -\epsilon \partial \beta_B(t)/\partial t, \quad (27)$$

where β_A and β_B are $1/kT_A$ and $1/kT_B$, respectively;

$$\epsilon = \text{Tr}(H_{rfB}^{*2})/\text{Tr}(H_{AA}^2) \simeq N_B/N_A (\gamma_B H_{1B}/\gamma_A h_L)^2 \quad (28)$$

is the ratio of the B and A heat capacities; and

$$\frac{\partial \bar{\beta}_A}{\partial t} = \left(\frac{\Delta V}{V}\right) \frac{\partial \bar{\beta}_{Ar_0}}{\partial t} + \left(\frac{V-\Delta V}{V}\right) \frac{\partial \bar{\beta}_{Ar}}{\partial t}. \quad (29)$$

The bar indicates a spatial average; the subscript r_0 indicates the spatial average over a volume ΔV out to radius r_0 , where

$$\Delta V = \frac{4}{3}\pi r_0^3, \quad (30)$$

and the subscript r indicates the volume average from r_0 to $\frac{1}{2}r_{BB}$. The first term on the right of Eq. (29) is the weighted average of $\partial \beta_A(\mathbf{r}, t)/\partial t$ over the region where A and B nuclei interact directly via dipolar coupling. In this region the phenomenological diffusion equation⁸ can be written as

$$\frac{\partial \bar{\beta}_{Ar_0}}{\partial t} \simeq \left(\frac{V\epsilon W_{AB}}{\Delta V}\right) (\beta_B - \bar{\beta}_{Ar_0}) + \left(\frac{4\pi D r_0^2 V}{\Delta V}\right) \frac{\partial \beta_A}{\partial r} \Big|_{r_0}. \quad (31)$$

The first term in (31) is the driving term caused by the externally rf-excited B nuclei, and the second term represents diffusion through a spherical surface into the region ΔV from the bulk A nuclei at radius r_0 , according to Fick's law. The choice of r_0 is somewhat arbitrary. It is defined as a mean radius at which the direct dipolar coupling between B and neighboring A spins at $r=r_0$ falls off to a value such that $\partial \bar{\beta}_{Ar}/\partial t$ in (29) depends only on $(\partial \beta_A/\partial r)|_{r_0}$; namely where β_{Ar} is affected by spin diffusion and not by negligibly weak A - B dipolar interactions. In principle r_0 has a

⁸ N. Bloembergen, *Physica* **15**, 386 (1949).

slow time dependence upon $(\partial\beta_A/\partial r)|_{r_0}$, but the crudeness of this model does not justify further refinement beyond the assignment of a time-averaged empirical value to r_0 . W_{AB} is identified as the coupling rate of B to A and is expressed in this model as

$$W_{AB} = \frac{4\pi C}{V} \int_{\Delta V} \frac{r^2 dr}{r^6} \approx \frac{1}{T_{AB}'} = \frac{T_{AA}}{T_{AB}^2}, \quad (32)$$

with

$$T_{AB}' = T_{AB}(T_{AB}/T_{AA}), \quad (33)$$

where T_{AB} is of the order of the A - B spin-flip time, T_{AA} is the A - A mutual spin-flip time, and C is of the order of $\hbar^2\gamma_A^2\gamma_B^2N_A T_{AA}$. W_{AB} can be approximated in more detail using the density-matrix master-equation approach,^{3,6,9} but an order-of-magnitude estimate is all that is relevant to this model and our experimental results. It is assumed here that the resonance condition, Eq. (1), is satisfied. D in Eq. (31) is the A -spin diffusion constant, approximated by⁸

$$D \cong a^2/50T_{AA},$$

where a is the internuclear spacing. The A nuclei far removed from the B nuclei become disordered, in terms of the reciprocal temperature β_A , at an average rate

$$\partial\bar{\beta}_A/\partial t = -[4\pi D r_0^2/(V-\Delta V)](\partial\beta_A/\partial r)|_{r_0}, \quad (34)$$

and the B nuclei increase in order at a rate

$$\partial\beta_B/\partial t = W_{AB}(\bar{\beta}_A - \beta_B). \quad (35)$$

The double-resonance-coupling and spin-diffusion process within the spherical volume bounded by radius $\frac{1}{2}r_{BB}$ defines the cell geometry of this phenomenological model. It has been assumed that

$$(\partial\beta_A/\partial r)|_{r_{BB}/2} = 0 \quad \text{at} \quad r = \frac{1}{2}r_{BB}, \quad (36)$$

as shown in Fig. 4. β_A can be related to the gradient of β_A at r_0 using Eqs. (27), (31), (29), and (34), yielding

$$\frac{\partial^2\beta_A}{\partial r \partial t} \Big|_{r_0} \frac{4\pi r_0^2 D}{\Delta V} = -\epsilon^{-1} \left[\frac{1}{W_{AB}} \frac{\partial^3\beta}{\partial t^3} + \frac{\partial^2\beta}{\partial t^2} \left(1 + \frac{\epsilon V}{\Delta V} \right) \right]. \quad (37)$$

β_A can be expanded in a Taylor series about r_0 , as

$$\beta_A(r, t) = \beta_A(t)|_{r_0} + (r-r_0)(\partial\beta_A/\partial r)|_{r_0} + \frac{1}{2}(r-r_0)^2(\partial^2\beta_A/\partial r^2)|_{r_0} + \dots, \quad (38)$$

where only the first three terms shown will be retained. Using Eqs. (37), (34), and (36), the rate equation of interest is obtained as

$$\frac{\partial^3\bar{\beta}_A}{\partial t^3} + \frac{\partial^2\bar{\beta}_A}{\partial t^2} \left[W_{AB} \left(1 + \frac{\epsilon V}{\Delta V} \right) + \frac{D}{G(V-\Delta V)} \right] + \frac{D}{G} \frac{W_{AB}(1+\epsilon)V}{(V-\Delta V)} \frac{\partial\bar{\beta}_A}{\partial t} = 0, \quad (39)$$

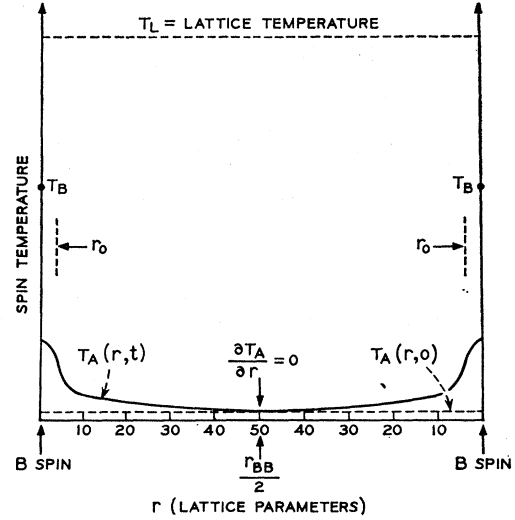


FIG. 4. Model used to estimate double-resonance relaxation rate. Concentration of B nuclei is 10^{-6} of A nuclear concentration. B nuclei interact directly with A nuclei out to a radius r_0 . Temperature for $r > r_0$ is nonuniform because of spin diffusion among A nuclei. $T_B > T_A$ is maintained by 180° phase shifts of the rf field.

where

$$G = (\Delta V/r_0^2) \left((V-\Delta V)^{-1} \int_{r_0}^{r_{BB}/2} r^2 dr \mathfrak{F}(r) - V^{-1} \int_0^{r_0} r^2 dr \mathfrak{F}(r) \right), \quad (40)$$

and

$$\mathfrak{F}(r) = (r-r_0) - [(r-r_0)^2/(r_{BB}-2r_0)]. \quad (41)$$

For the case of interest where $N_B \ll N_A$, then $r_0 \ll r_{BB}$, and

$$G \cong (3/40)r_0 r_{BB}. \quad (42)$$

Equation (39) simplifies in two limits of the parameter

$$D/GW_{AB} \cong 4a^2 T_{AB}^2 / 15r_0 r_{BB} T_{AA}^2. \quad (43)$$

If $D/r_0 r_{BB} \gg W_{AB}$, spin diffusion among A nuclei is sufficiently rapid to maintain a spatially uniform spin temperature for A nuclei, and there is no diffusion limiting for transfer of disorder between A and B nuclei. However, a diffusion bottleneck might be expected when $W_{AB} \gg D/r_0 r_{BB}$, since A nuclei near the B nuclei will disorder more rapidly than more distant nuclei. For parameters typical of experiments described here,

$$W_{AB} \cong 2 \times 10^8 \text{ sec}^{-1} \quad \text{and} \quad D/r_0 r_{BB} \cong 1 \text{ sec}^{-1},$$

so that the diffusion-bottleneck limit is of interest.

First consider the simple case for $D/r_0 r_{BB} \gg W_{AB}$, where Eq. (39) simplifies to

$$\partial^2\beta_A/\partial t^2 = -W_{AB}(1+\epsilon)\partial\beta_A/\partial t. \quad (44)$$

The average bars have been dropped, since a uniform spin temperature is assured for this case. Using Eq.

⁹ R. E. Slusher, Ph.D. thesis, University of California, Berkeley, Calif. (unpublished).

(27),

$$\beta_A(t) = \beta_{Ai} \{ 1 - \epsilon [1 - \beta_{Bi} / \beta_{Ai}] [1 - \exp(-tW_{AB}(1+\epsilon))] \} \quad (45)$$

where the subscript i signifies initial value. Equation (45) applies during each period between 180° phase shifts of H_{1B} . Immediately after a 180° phase shift

$$\beta_{Bi} = -\beta_B^-, \quad (46)$$

where β_B^- is the reciprocal B -spin temperature immediately before the phase shift. After n phase shifts, each separated by τ seconds,

$$\beta_A(n\tau) \cong \beta_A(0) (1 - \epsilon\alpha\delta)^n, \quad (47)$$

where α becomes constant at some value in the range

$$0 < [\alpha = (1 + \beta_B^- / \beta_{Ai})] < 2, \quad (48)$$

and

$$\delta = 1 - \exp[-\tau W_{AB}(1+\epsilon)]. \quad (49)$$

For large n and small ϵ ,

$$\beta_A(n\tau) \cong \beta_{A0} \exp(-n\epsilon\alpha\delta). \quad (50)$$

Equation (50) is the optimum double-resonance rate expected, and the decay constant at resonance is of the order of ϵW_{AB} , which predicts detectability of as few as $N_B \cong 10^{-7} N_A$, if the A nuclear-resonance signal can be detected with a signal-to-noise ratio of $10^2:1$, and the low-field spin-lattice relaxation time permits coupling the A and B nuclei for a period of the order of 100 sec. This sensitivity is comparable with other double-resonance techniques.^{3,5,6} It is interesting to write explicitly the dependence of the double-resonance rate on H_{1B} . The quantity W_{AB} can be shown^{3,9} to vary as

$$W_{AB} \cong (T_{AA}/T_{AB}^2) \exp[-3(\gamma_B H_{1B} T_{AA})^2], \quad (51)$$

for H_{1B} much larger than the A - B dipolar interactions; and substituting t for $n\tau$ one obtains

$$\ln[\beta_A(t)/\beta_A(0)] \cong -H_{1B}^2(\alpha t/\tau) (\gamma_B/\gamma_A h_L)^2 (N_B/N_A) \{ 1 - \exp[-(\tau T_{AA}/T_{AB}^2) \exp(-3(\gamma_B H_{1B} T_{AA})^2)] \}. \quad (52)$$

Notice that the double-resonance rate is optimum for resonance condition Eq. (1), and decreases rapidly for larger H_{1B} as the exponential factor begins to dominate.

Finally, consider the double-resonance relaxaton for slow spin diffusion, $D/r_0\sigma_{BB} \ll W_{AB}$, for which Eq. (39) becomes

$$\frac{\partial^3 \bar{\beta}_A}{\partial t^3} + \frac{\partial^2 \bar{\beta}_A}{\partial t^2} W_{AB} \left(1 + \frac{\epsilon V}{\Delta V} \right) + \frac{D}{G} W_{AB} \frac{\partial \bar{\beta}_A}{\partial t} = 0. \quad (53)$$

Using Eq. (27), the following set of equations are obtained:

$$\bar{\beta}_A = K [\exp(m_+\tau) - \exp(m_-\tau)] + \frac{\bar{\beta}_{Ai} - \epsilon \beta_B^-}{1+\epsilon} + \epsilon \left(\frac{\bar{\beta}_{Ai} + \beta_B^-}{1+\epsilon} \right) \exp(m_-\tau), \quad (54)$$

where

$$m_+ = -(D/4G) (1 + \epsilon V/\Delta V)^{-1},$$

$$m_- = -W_{AB} (1 + \epsilon V/\Delta V),$$

and

$$K = \frac{\epsilon W_{AB}}{(1+\epsilon)(1+\epsilon V/\Delta V)} \left(\frac{\bar{\beta}_{Ai}(1+\epsilon V/\Delta V) - \bar{\beta}_{Ar_0i}(1+\epsilon) + \beta_B^- \epsilon [(V-\Delta V)/\Delta V]}{W_{AB} - (D/4G)(1+\epsilon V/\Delta V)^{-2}} \right);$$

$$\beta_B = -\beta_B^- + (1/\epsilon) (\bar{\beta}_{Ai} - \bar{\beta}_A); \quad (55)$$

and

$$\bar{\beta}_{Ar_0} = (K/\epsilon W_{AB}) [m_- \exp(m_-\tau) - m_+ \exp(m_+\tau)] + [(\bar{\beta}_{Ai} - \bar{\beta}_A)/\epsilon] - \beta_B^- + [(\bar{\beta}_{Ai} + \beta_B^-)/(1+\epsilon)] (1 + \epsilon V/\Delta V) \exp(m_-\tau). \quad (56)$$

Equations (54), (55), and (56) apply during each period between 180° phase shifts. Together with initial conditions at the beginning of the experiment, they form a complete set of equations necessary for describing $\bar{\beta}_A$, β_B , and $\bar{\beta}_{Ar_0}$ throughout the experiment, as 180° phase shifts, n in number, are applied in periodic fashion. Figure 5 shows computer plots of the envelope of $\bar{\beta}_A$ as a function of over-all time $t = n\tau = \tau_0$, for various values of τ , $\Delta V/V$, and D . ϵ was taken as 10^{-6} and W_{AB} as $2 \times 10^8 \text{ sec}^{-1}$, typical for experiments described here for NaCl. The initial A -spin temperature

was taken as 0.01°K after adiabatic demagnetization, and the B -spin temperature was initially infinite. For ϵ of 10^{-6} , $r_{BB} \approx 100a$, and

$$\Delta V/V \cong (r_0/50a)^3.$$

r_0 is expected to be of the order of a few lattice parameters because of the A - B dipolar interaction. Solutions for $\bar{\beta}_{Ar_0}$ (not shown) reveal that for smaller values of $\Delta V/V$ and D , the A nuclei near the B spin heat up during the initial relaxation period and limit the rate at which the B nucleus can disorder the A nuclei. This

diffusion-bottleneck behavior is seen in the initial curvature of the relaxation in Fig. 5. These solutions show that for ϵ in the 10^{-6} range the diffusion bottleneck is not expected to decrease the double-resonance relaxation rate by more than an order of magnitude.

C. Rotary Saturation by Frequency Modulation

Frequency modulation of H_{1B} has proved to be a more versatile method for continuously disordering the B nuclei. This method is similar to a rotary-saturation technique of Redfield,¹⁰ which uses audio-frequency fields to saturate the nuclear magnetization along a high-frequency rf field. Audio-frequency rotary saturation has been used for nuclear double resonance.^{5,6} However, in zero field, an audio-frequency field would saturate and disorder the A nuclei, since the audio frequency required, $\gamma_B H_{1B}$, is of the order of $\gamma_A \hbar L$. We will now show that this impasse can be avoided by using an effective audio-frequency field caused by modulating the frequency of H_{1B} about the quadrupole-resonant frequency ω_Q , as expressed by

$$\omega_B = \omega_Q + \Delta\omega \cos \omega_M t, \quad (57)$$

where ω_M is the modulation frequency, and $\Delta\omega$ is the frequency deviation. The effective field H_M is defined as

$$2H_M \gamma_B \equiv \Delta\omega. \quad (58)$$

Integrating (57) we find

$$H_{1B}(t) = H_{1B}^0 \cos(\omega_Q t + m \sin \omega_M t), \quad (59)$$

where

$$m = \Delta\omega / \omega_M \quad (60)$$

is the modulation index. In order to transform out the time dependence of H_{1B} , we use the unitary transformation

$$U_Q = \exp\left\{-\frac{1}{\hbar} i(\omega_Q t + m \sin \omega_M t) \sum_j [3S_{zj}^2 - \mathbf{S}_j^2]\right\} \quad (61)$$

in place of the transformation Eq. (20). The interaction representation Hamiltonian becomes

$$H^* = -\hbar H_M \gamma_B \cos \omega_M t$$

$$\times \sum_j^B [3S_{zj}^2 - \mathbf{S}_j^2] + H_{AA} + H_{rtB}^* + H_{AB}^*, \quad (62)$$

where we have assumed that H_M is much less than local dipole fields and H_{1B} . For a single B -spin we can write the Hamiltonian

$$h_B^* = h_{rtB}^* + h_{AB}^* + h_M^*, \quad (63)$$

where

$$h_M^* = -\frac{1}{2} \hbar H_M \gamma_B [\exp(i\omega_M t) + \exp(-i\omega_M t)] \times [S_z^2 - S(S+1)]. \quad (64)$$

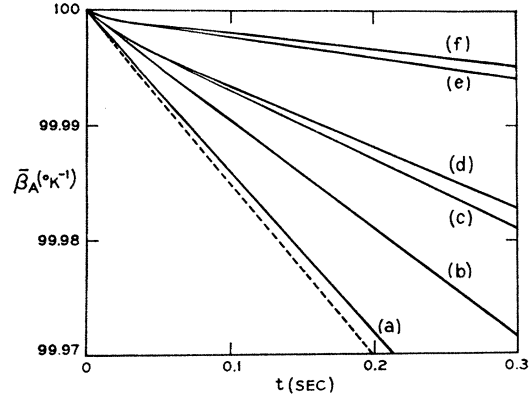


FIG. 5. Computer plots of envelope of β_A as a function of overall time $t = n\tau$. The double-resonance relaxation applies for 180° phase shifts applied at a period of τ seconds, where the sequence occurs n times in a measurement. Parameters in the range of interest for the experiments described here are (a) $\tau = 1$ msec, $(\Delta V/V) = (2/50)^3$, $(D/4G) = 1$; (b) $\tau = 1$ msec, $(\Delta V/V) = (1/50)^3$, $(D/4G) = 1$; (c) $\tau = 2$ msec, $(\Delta V/V) = (2/50)^3$, $(D/4G) = 10$; (d) $\tau = 2$ msec, $(\Delta V/V) = (2/50)^3$, $(D/4G) = 0.1$; (e) $\tau = 2$ msec, $(\Delta V/V) = (1/50)^3$, $(D/4G) = 10$; (f) $\tau = 2$ msec, $(\Delta V/V) = (1/50)^3$, $(D/4G) = 0.1$. Notice the initial curvature away from the dashed line (no diffusion-limiting case) resulting from local heating of A nuclei near the B nucleus, as shown in Fig. 4.

First-order perturbation theory¹¹ can now be used for h_M^* to show that frequency modulation disorders the B nuclei at a rate

$$1/\tau_M = 8H_M^2 \gamma_B^2 T_{AB}' \quad (65)$$

for the resonance condition,

$$\omega_M = \sqrt{3}\omega_{1B} \quad (66)$$

[see eigenvalues of Eq. (24)]. In order to maintain the B nuclei in a state of maximum disorder, we require

$$\tau_M \cong T_{AB}'. \quad (67)$$

This effective rotary-saturation technique makes it possible to determine the γ_B of the B nucleus, since H_{1B} and the resonance value [Eq. (60)] of ω_M can be measured. H_{1B} is the projection of the applied rf field on a plane perpendicular to the z principal axis. Therefore, if γ_B is known and η is zero, the orientation of the electric field gradient principal axis can be determined by rotating the polarization of H_{1B} . If η is nonzero, B spin energy-level spacings in the interaction representation differ from those of Eq. (24), as shown in the Appendix. The accuracy for determining γ_B , H_{1B} , or the field-gradient orientation depends on the B -spin interaction representation linewidth, which is determined by H_{AB}^* or inhomogeneous electric field gradients.

For a static deviation of H_{1B} frequency from the B -spin quadrupole resonance by an amount Δ , the effective Hamiltonian in the interaction representation

¹⁰ A. G. Redfield, Phys. Rev. **98**, 1787 (1955).

¹¹ A. Abragam, *The Principles of Nuclear Magnetism* (The Clarendon Press, Oxford, England, 1961), p. 40.

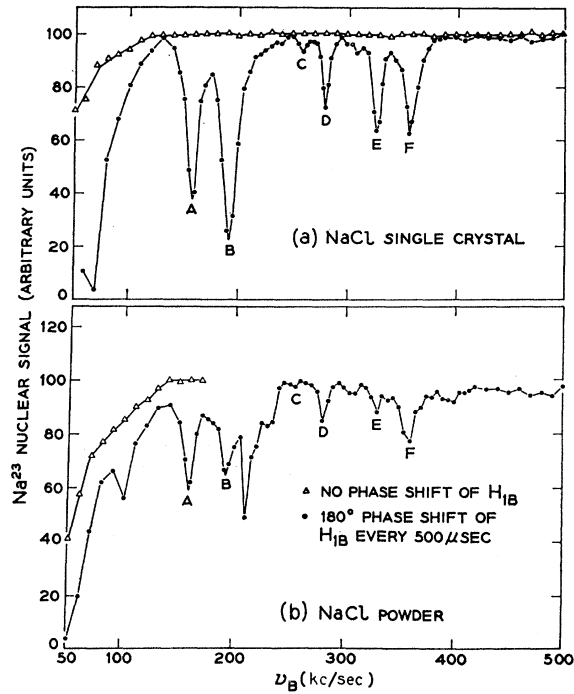


FIG. 6. Nuclear-quadrupole-resonance spectra for commercial-purity NaCl, using 180° phase shifts of H_{1B} . Each rotating component of H_{1B} was approximately 2 G. A single crystal from the Harshaw Chemical Company with H_{1B} parallel to the (100) direction is shown in (a). Spectrum of reagent-grade powder ($100\text{--}150\mu$) is shown in (b). Both samples were at liquid-nitrogen temperature.

for a single B spin is

$$h_B^*(\Delta) = h_\Delta^* + h_{rf B}^* + h_{AB}^* + h_M^*, \quad (68)$$

where

$$h_\Delta^* = \frac{1}{6}(\hbar\Delta)[3S_z^2 - S(S+1)]. \quad (69)$$

Considering h_M^* and h_{AB}^* as small perturbations, $h_B^*(\Delta)$ can be diagonalized, and one finds the eigenvalues

$$E = \pm \frac{1}{2}\hbar(\Delta^2 + 3\omega_{1B}^2)^{1/2}. \quad (70)$$

Frequency modulation (fm) now causes maximum disorder for B nuclei when the resonant condition

$$\omega_M = (\Delta^2 + 3\omega_{1B}^2)^{1/2} \quad (71)$$

is obtained.

III. EXPERIMENTAL RESULTS

A. Experimental Apparatus

As indicated in Fig. 3, the sample and rf coils are mounted in a 10-liter Dewar filled with liquid nitrogen and mounted between the poles pieces of a 10-kG electromagnet. Timing of the entire cycle (Fig. 1) is automatically controlled by a series of Tektronix 160-series waveform generators. First, the sample is polar-

ized in the 10-kG field for a period of the order of T_1 (typically 1 to 10 min). After polarization the sample is pulled to a zero-field region above the magnet by a nylon rod attached to a small elevator mechanism [time points (a) to (b) on Fig. 1]. A Helmholtz coil is used to cancel any remaining fields to within ± 0.5 G over the volume of the sample. The sample slides freely in a bakelite tube which is wrapped with a solenoid used to generate the rf field H_{1B} . The solenoid is part of the tuned output load of a linear rf amplifier made up of a video amplifier and two parallel 813 tubes operating as a class A amplifier. Phase-shift or frequency modulation of H_{1B} is determined at the input of the video amplifier by a 180° electronic phase shifter or a fm signal generator. 180° phase shift is accomplished by transistor-switching from an anode-follower amplifier to a grounded grid amplifier, both using a 6DJ8 dual triode tube. H_{1B} is applied to the sample for a fixed period in zero field, $t = \tau_0$, and the frequency of H_{1B} is fixed during each cycle but is changed in increments of from 0.1 to 10 kc/sec during each polarization period in high field. The magnetic order of the A nuclei decreases during the period in the zero-field region because of spin-lattice relaxation and cross-relaxation with the irradiated B nuclei. After τ_0 seconds in zero field, the sample is remagnetized by dropping it back into the 10-kG field, where the remaining A nuclear magnetization is measured by a 90° rf pulse (10 mc/sec for Na in NaCl and 40 mc/sec for protons) [time points (c), (d), and (e) in Fig. 1]. If H_{1B} is applied at the quadrupole resonance of a set of B nuclei, the measured magnetization is expected to vary as

$$M_z(\tau_0) = M_z(0) \exp\{-\tau_0[(1/T_{1d}) + (1/\tau_{AB})]\}. \quad (72)$$

This behavior is shown experimentally in Fig. 2. If the frequency of H_{1B} is off the B -quadrupole resonance, τ_{AB} is infinite and we therefore expect B -quadrupole resonances to appear as a dip in $M_z(\tau_0)$. Immediately after measuring M_z a series of twenty 90° pulses at 10-msec intervals is applied to completely saturate M_z to zero value.

B. Pure Quadrupole Spectra in Impure NaCl

NaCl single crystals were obtained from The Harshaw Chemical Company in the form of $\frac{1}{2}$ -in.-diam cylinders $1\frac{1}{2}$ in. long. NaCl powders were obtained commercially or crystallized from aqueous solution. Crystals were mounted in Teflon cylinders which slide between the high- and low-field region. For Na^{23} nuclei at liquid-nitrogen temperatures in both single crystals and powder, T_1 in a 10-kG field was about 300 sec. In the zero-field region (± 0.5 G), T_{1d} varied between 50 and 100 sec, depending on the purity of the sample. Na^{23} nuclei were used as the A nuclei in hope of detecting quadrupole interactions of Na and Cl nuclei at noncubic sites near imperfections and impurities. Using the 180° phase-shift method the spectrum in

Fig. 6 was obtained for commercial-quality NaCl single crystals and powders. Other resonances found in large single crystals but not shown were at 560 and 820 kc/sec. Searches extended up to 1.5 mc/sec. The 180° phase shift occurred during a period Δ_s (typically 50 to 100 μ sec), which varied with the Q of the B_{rf} circuit. If Δ_s is too short, sidebands are produced which broaden the observed resonances. If Δ_s is too long, the phase shift will be adiabatic for the B nuclei, and B -spin disorder will not be maintained.

Commercial powders were found to have spectra similar to large single crystals, but with a few additional resonances. Relative intensities of various resonances depended on the commercial source. Since cubic symmetry is destroyed at crystal surfaces, the number of B nuclei with quadrupole interactions ($\sim 10^{17}$ cm $^{-3}$) is in the observable range for 100 μ cubic crystals. After the single crystal, which provided the data for Fig. 6, was crushed into small crystals (50 to 100 μ), small resonances appeared at 100 and 125 kc/sec, while other resonances remained unchanged. The 100-kc/sec resonance appeared in all powders and never in large single crystals; therefore, it may be associated with surfaces, vacancies, grain boundaries, or cracks. None of the other resonance intensities changed appreciably with crystal size. Absorption below 100 kc/sec is caused by direct nuclear absorptions from low-frequency quadrupole- and dipole-coupled nuclei with energy levels which overlap from neighbor to neighbor.

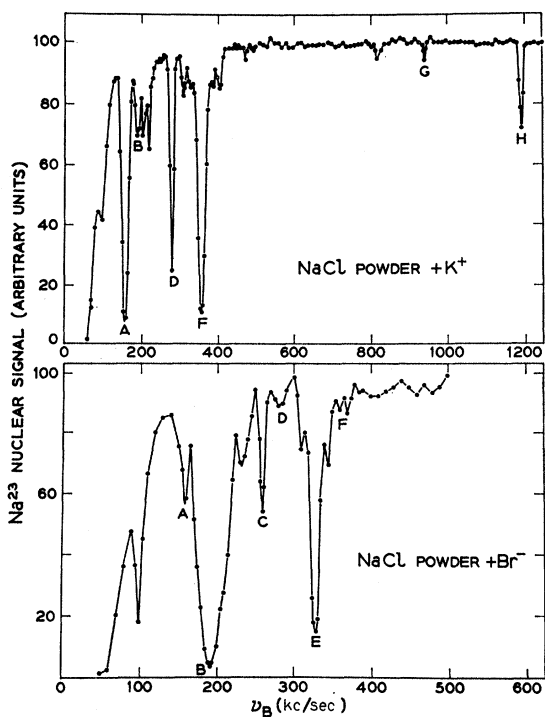


FIG. 7. Nuclear quadrupole resonance after adding K^+ (0.1 molar %) and Br^- (0.2 molar %). Experimental conditions are the same as in Fig. 6.

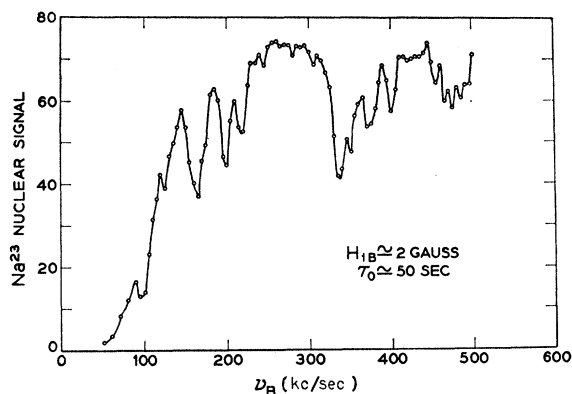


FIG. 8. Nuclear-quadrupole spectra after addition of Ca^{++} to NaCl. Experimental conditions are the same as in Fig. 6.

In order to identify the source of the electric field gradients responsible for the observed resonances, small crystals were grown from saturated NaCl solutions with various added impurities. All samples were annealed in vacuum. As shown in Fig. 7, resonances A , D , F , G , and H increased in intensity after adding K^+ . Resonances B , C , and E increased after adding Br^- . Other resonance intensities remained at the level found in reagent-grade NaCl, and a few new resonances appeared. Preliminary identifications² of the resonant nuclei were made from this data assuming the quadrupole frequency decreased with the distance from the substitutional impurity. Cl^{37} - Cl^{35} doublets can be identified because of their frequency ratio,¹² 1.27, determined by the ratio of their quadrupole moments. However, the frequency-modulation technique was later used, as discussed in Sec. IIIC, to show that these initial identifications were incorrect.

Other substitutional impurities such as Ag^+ , I^- , F^- , H^- , Li^+ , and Cs^+ would be interesting to study, but no attempts were made to grow crystals with these impurities. Divalent metallic ions caused a complicated spectra as shown in Fig. 8. Various charge-compensation configurations probably contribute to the width and complexity of the spectra. Quadrupole interactions near F centers and other paramagnetic impurities are probably not observable by this technique because of large contact and dipolar fields at neighboring nuclei caused by the unpaired electrons.

Unfortunately, it is difficult to determine the number of isolated substitutional impurities in NaCl. It is not known how many impurity ions from solution are included in the crystal or if impurities form clusters or migrate to grain boundaries. Annealing effects the observed resonances as shown in Fig. 9. An interesting resonance appears at 430 kc/sec for powders annealed in the atmosphere instead of vacuum. It has been shown¹³ that OH^- concentration increases when NaCl is heated in a moist atmosphere, which suggests that

¹² T. C. Wang, Phys. Rev. **99**, 566 (1955).

¹³ D. A. Otterson, J. Chem. Phys. **33**, 227 (1960).

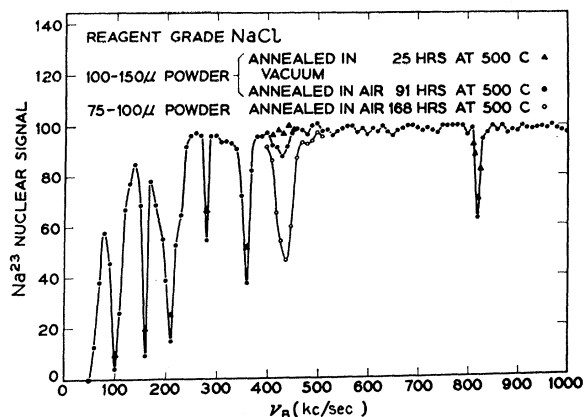


FIG. 9. Effects of annealing on quadrupole spectra. Experimental conditions are similar to those of Fig. 6.

the 430-kc/sec resonance is a Na nucleus near a OH⁻ substitutional ion.

Figure 10 shows the *A*-spin signal after a fixed period in zero field as a function of H_{1B} . Equation (52) predicts an H_{1B}^2 dependence for H_{1B} small compared to the *A* dipolar fields. This initial slope, which was observed as shown in Fig. 10, can be used to estimate the number of *B* nuclei. Table I shows the density of Cl³⁵ nuclei (*B* spins) estimated using Eq. (52) and Fig. 10. The site of this quadrupole resonance we show to be located at coordinates (111) from the K⁺ substitutional ion, where symmetry requires the asymmetry parameter η to be zero. Thus the effective H_{1B} field is well defined and can be measured experimentally as shown in the following section. N_K , the density of K⁺ ions, is $\frac{1}{6}N_B$, since these are six Cl³⁵ neighbors con-

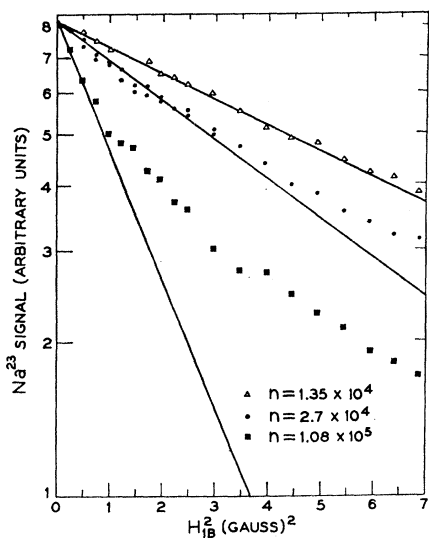


FIG. 10. *A*-spin signal as a function of H_{1B} and τ for Cl³⁵ nuclei at a (111) position from a K⁺ substitutional ion. ν_Q was 280 kc/sec. H_{1B} is aligned along the (111) axis of the single-crystal sample. n is the number of 180° phase shifts during a 54-sec period in zero field. Solid lines show initial slopes used to estimate density of K⁺ ions in crystal.

tributing to the resonance for H_{1B} parallel to the (111) direction.

Notice that the initial slopes decrease with increasing τ . Assuming fast spin diffusion, Eq. (52) shows that this behavior provides a measure of T_{AB}' . For these data, T_{AB}' is of the order of 500 μ sec which is in the range of 200 μ sec, expected from the T_{AA} for NaCl in high field. However, these data do not resolve whether or not spin diffusion plays a role in the relaxation rate. It is difficult to determine N_K independently, and it is not known to what degree the impurities tend to cluster. N_K might be larger than the estimates of Table I if spin diffusion decreases the relaxation rate. However, as seen in Fig. 5, the theoretical estimates for spin-diffusion limiting are not large in this range of concentrations ($\epsilon \sim N_B/N_A \sim 10^{-5}$ to 10^{-6}). Also, for the Harshaw single crystals, N_K is expected to be in the range from 10^{15} to 10^{17} cm⁻³. Finally, note that the exponential H_{1B} dependence of Eq. (52) becomes evident in Fig. 10 at fields of 1 to 2 G, which is in good agreement with a calculated value [Eq. (14)] of 1.3 G for h_L in zero field for NaCl.

TABLE I. Estimated density of quadrupole coupled Cl³⁵ nuclei N_B near K⁺ ions.

n	τ (msec)	N_B (cm ⁻³)	N_K (cm ⁻³)
1.35×10^4	4	2.6×10^{18}	4.3×10^{17}
2.7×10^4	2	2×10^{18}	3.3×10^{17}
1.08×10^5	0.5	1.7×10^{18}	2.7×10^{17}

C. Identification of Quadrupole Resonances by Frequency Modulation

B nuclei can be maintained in a magnetically disordered state if ω_B is frequency-modulated about ω_Q , as shown in Sec. IIC. The experimental parameters of interest are the magnitude [H_M of Eq. (58)] and resonance frequency [ω_M of Eq. (66)] of modulation. For NaCl the requirements are $\omega_M/2\pi$ in the range from 2 to 10 kc/sec and $\Delta\omega$ of about 1 kc/sec. Frequency-modulated *B* rf was generated by a 10-mc/sec fm generator. This signal was mixed with an unmodulated signal at 10 mc/sec plus ν_B to obtain the difference frequency ν_B modulated in the same manner as the 10-mc/sec fm signal. Frequency deviation $\Delta\omega$ was not measured accurately but was held constant at near 0.1-kc/sec for all data. ω_M was determined by the audio oscillator input to the fm generator.

The shape of the quadrupole resonance depends on ν_M as shown in Fig. 11. This is the behavior predicted by Eq. (71). For ω_M greater than $\sqrt{3}\gamma_B H_{1B}$, there are two resonances at

$$\omega = \omega_B \pm (\omega_M^2 - 3\omega_{1B}^2)^{1/2}. \quad (73)$$

If ω_M is less than $\sqrt{3}\gamma_B H_{1B}$, there is a single resonance that decreases in intensity as ω_M decreases. If we fix

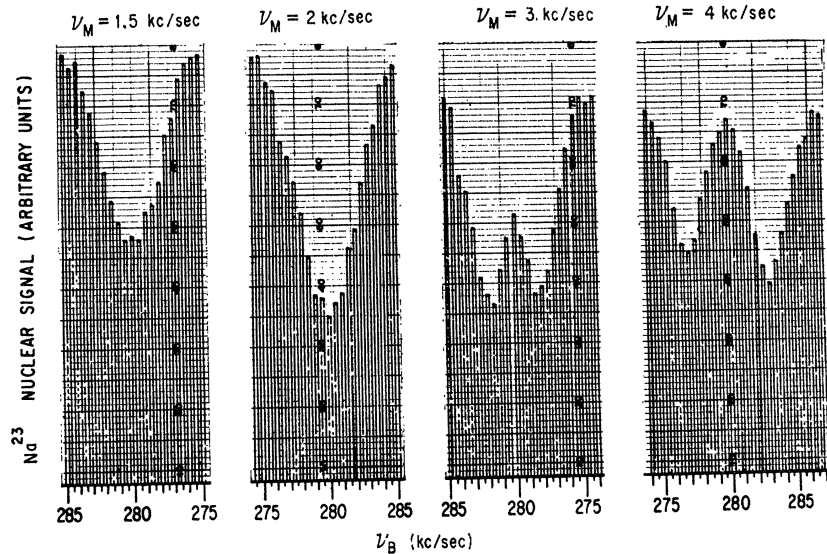


FIG. 11. Cl^{35} quadrupole resonance at $\nu_Q = 280$ kc/sec using frequency modulation.

the frequency of H_{1B} at ω_Q and vary ω_M , we expect the resonance of Eq. (66). Figures 12 and 13 show several ω_M resonances for Na and Cl neighbors of K^+ and Br^- nuclei. We can now definitely identify the source of each resonance. Resonances (a) and (b) in Fig. 12 are identified as Cl^{37} and Cl^{35} , respectively, since

$$\frac{\nu_M(\nu_Q = 220 \text{ kHz})}{\nu_M(\nu_Q = 280 \text{ kHz})} = 0.81 \pm 0.2 \sim \frac{\gamma_{\text{Cl}^{37}}}{\gamma_{\text{Cl}^{35}}} = 0.83, \quad (74)$$

and the quadrupole-frequency ratio is 1.27 as expected. Similarly, the high-frequency resonances G and H are also a Cl^{37} - Cl^{35} pair, and because of their high frequency they are identified as K^+ -Cl(1, 0, 0) sites. The 220-280-kc/sec Cl doublet is then a K^+ -Cl(1, 1, 1) site.

TABLE II. Rare quadrupole resonances in NaCl.

Resonance	Resonance frequency ν_B (kc/sec)	Impurity center	Resonant neighbor nucleus
	70
	100
	125
A	158	K^+	Na^{23} (1, 1, 2)
B	191.5	Br^-	Na^{23}
	205	...	Na^{23}
	210	...	Na^{23}
	220	K^+	Cl^{37} (1, 1, 1)
C	259	Br^-	Cl^{37} (?)
D	280	K^+	Cl^{35} (1, 1, 1)
	310
E	328.5	Br^-	Cl^{35} (?)
F	358	K^+	Na^{23} (1, 1, 0)
	430
	580	...	Na^{23}
	821
G	944.5	K^+	Cl^{37} (1, 0, 0)
H	1197	K^+	Cl^{35} (1, 0, 0)

Symmetry requires both (1, 0, 0) and (1, 1, 1) sites to be axially symmetric; therefore, Eq. (66) applies, and we can determine the effective value of H_{1B} as 2.84 ± 0.05 G. The effective component of H_{1B} is perpendicular to the z principal axis of the electric field gradient, which symmetry requires to lie along the $\langle 111 \rangle$ direction. Since H_{1B} was applied along the

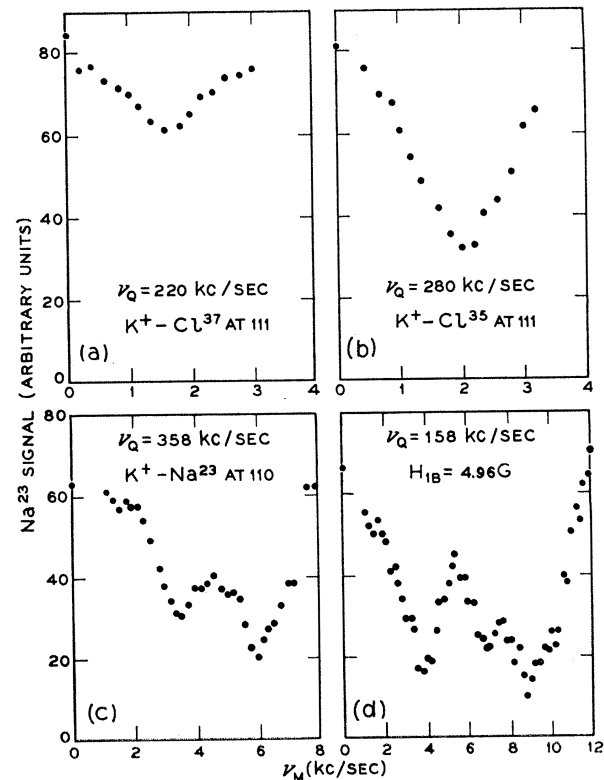


FIG. 12. Na and Cl resonances near K^+ substitutional ions as a function of modulation frequency ν_M . ν_B was fixed at ν_Q . Irradiation period $t = \tau_0$ in zero field was 54 sec.

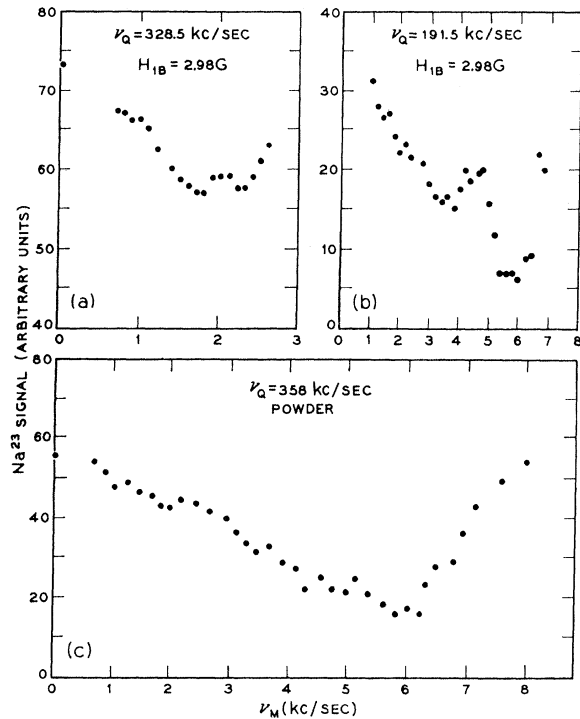


FIG. 13. Na and Cl resonances associated with addition of Br are shown in (a) and (b) as a function of modulation frequency ν_M . A powder with 0.1 molar % K^+ is shown in (c); the ν_M resonance should be compared with Fig. 12(c).

$\langle 111 \rangle$ direction for all data for this section, geometry requires [see Fig. 14(a)] that the effective component of H_{1B} is

$$H_{1B\perp} = \frac{2}{3}\sqrt{2}H_{1B}.$$

Thus we obtain an applied field of 3.02 G from the ν_M resonance. This compares with 3.3 ± 0.5 G measured from the voltage induced in a small search coil. Two other resonances, at 158 and 258 kc/sec, were observed to increase with the addition of K^+ . As shown in Fig. 12(c), there are two ν_M resonances for ν_B fixed at the 358-kc/sec quadrupole resonance. This ν_B resonance is obviously Na^{23} , since the ν_M resonance is too high for the chlorine isotopes. The effective values of H_{1B} are 3 and 1.73 G. If we assume that the z principal axis at $(1, 1, 0)$ sites is along the $\langle 110 \rangle$ direction and the field gradient is axially symmetric, we obtain two inequivalent sites [see Fig. 14(b)]. H_{1B} of 3 G is applied along the $\langle 111 \rangle$ direction, and we obtain effective values of 3 and 1.73 G, which are in excellent agreement with the data. However, a $(1, 1, 0)$ -site symmetry does not require an axially symmetric field gradient, and one should perform orientation experiments using the results of the Appendix to confirm the orientation and asymmetry parameter for this site. The resonance at 158 kc/sec is also obviously Na^{23} , from the spectrum in Fig. 12(d). However, there are clearly three inequivalent sites, which eliminates the $(0, 0, 2)$ site and

suggests that the resonance may be caused by $(1, 1, 2)$ sites. The three resonances lie close to the values expected for a $(1, 1, 2)$ site assuming axial symmetry and a radial direction for the z principal axis, but these properties are certainly not required for electric field gradients at these distant sites. Note that one can distinguish the Na resonance in a powder where $H_{1B\perp}$ is random, as shown in Fig. 13(c).

Resonances which increased with addition of Br are quite enigmatic. The resonance at 328.5 kc/sec was thought² to be a Cl^{35} $(1, 1, 0)$ site near a Br^- ion. However, its ν_M spectrum [Fig. 13(a)] obviously does not compare with the Na $(1, 1, 0)$ site near K^+ . Even more surprising is the ν_M spectrum for the resonance at 191.5 kc/sec [Fig. 12(b)], which is almost identical to the Na $(1, 1, 0)$ resonance for Na near K^+ . However, the only possible sites for Na near an isolated Br^- substitutional ion are $(1, 0, 0)$, $(1, 1, 1)$, and $(1, 0, 2)$. If the 191.5-kc/sec resonance were the $(1, 0, 2)$ site, there should be other higher-frequency quadrupole resonances for the $(1, 0, 0)$ and $(1, 1, 1)$ sites, but none was found. It can not be a $(1, 0, 0)$ or $(1, 1, 1)$ site, since symmetry requires only one ν_M resonance for each of these sites. Suggestions for the source of these resonances are discussed in Sec. IV.

Table II summarizes the quadrupole resonances observed to date by this zero-field double-resonance

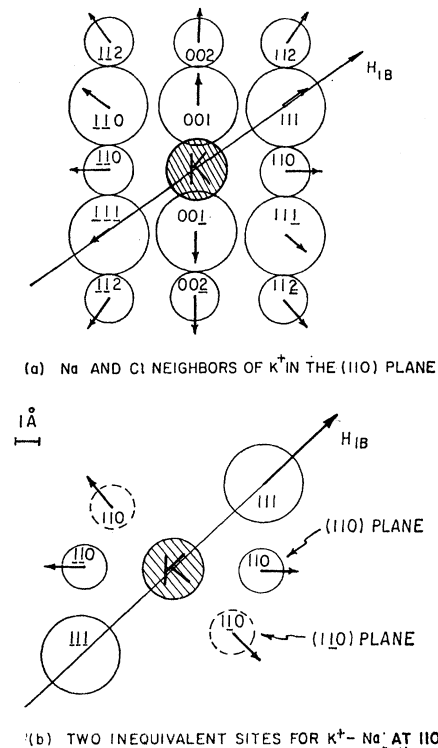


FIG. 14. Ionic arrangements near a K^+ substitutional ion showing the effective components of H_{1B} perpendicular to the electric field gradient z axis (assumed radial and indicated by arrows).

technique. In addition to those listed, there are the complex resonances seen after addition of Ca^{++} and high concentrations ($>1\%$) of Br^- and K^+ . Small resonances were often seen in the range from 400 to 500 kc/sec. It is obvious there is much to be learned about the observed spectra and many interesting impurity centers not yet studied.

D. Zero-Field Double Resonance in Proton Solids

Protons in solids seem to be an excellent A -spin system for nuclear double resonance because they have no quadrupole interaction, large magnetic resonance signals, and strong dipolar coupling. Proton magnetic resonance in solids with no internal motions is sometimes experimentally difficult because of the broad homogeneous linewidth caused by strong dipolar coupling. For example, in $\text{CaSO}_4 \cdot 2\text{H}_2\text{O}$ (gypsum) and C_{10}H_8 (naphthalene), the free-induction decay-time constant is in the range from 5 to 50 μsec at liquid-nitrogen temperature. For zero-field double-resonance experiments, one must usually work at liquid-nitrogen temperature or below to freeze out hindered rotations and other internal molecular motions which make the ratio $T_1(H_0)/T_{1d}$ so high that cycle time exceeds the patience of the experimenter. This ratio should be as small as possible. For $\text{CaSO}_4 \cdot 2\text{H}_2\text{O}$ (gypsum) and C_{10}H_8 (naphthalene) at 77°K , $T_1(H_0)$ is determined by paramagnetic impurities or molecular motions near impurity centers. For experiments described here we used polycrystalline U.S.P.-grade naphthalene and natural single crystals of $\text{CaSO}_4 \cdot 2\text{H}_2\text{O}$ from Ward Geological Supply irradiated in a Co^{60} source to introduce OH^- paramagnetic centers. The following relaxation times were found at liquid-nitrogen temperature:

	$\text{CaSO}_4 \cdot 2\text{H}_2\text{O}$	C_{10}H_8
$T_1(H_0=10 \text{ kG})$ (sec)	500	32
$T_{1d}(H_0 < h_L)$ (sec)	15	18.5

Interesting B systems for the solids above include D (natural abundance, 0.015%), S^{33} (0.74%), and O^{17} (0.03%). Deuterium quadrupole resonances are expected in the range from 50 to 200 kc/sec¹⁴ in C_{10}H_8 and at 170 and 190 kc/sec for D_2O ^{15,16} molecules in $\text{CaSO}_4 \cdot 2\text{H}_2\text{O}$. Spin quenching¹⁷ may reduce the sensitivity for detecting deuterium by a factor of as great as 100. O^{17} quadrupole resonances are expected between 500 kc/sec and 5 mc/sec. Zero-field double resonance requires the resonance condition, Eq. (1) and maximum sensitivity is expected for H_{1B} of nearly 50 G for D

¹⁴ W. D. Phillips, J. C. Rowell, and L. R. Melby, *J. Chem. Phys.* **41**, 2551 (1964); D. M. Ellis and J. L. Bjorkstam, *Bull. Am. Phys. Soc.* **12**, 468 (1967).

¹⁵ C. J. Gabriel, Ph.D. thesis, University of California, Berkeley, Calif. (unpublished).

¹⁶ T. Chiba, *J. Chem. Phys.* **39**, 947 (1963).

¹⁷ G. W. Leppelmeier and E. L. Hahn, *Phys. Rev.* **141**, 724 (1966).

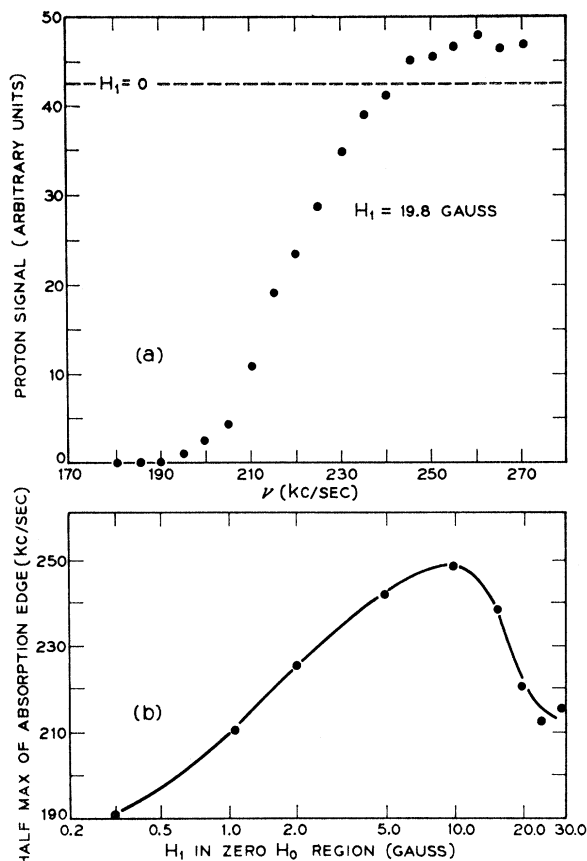


FIG. 15. Zero-field rf absorption for $\text{CaSO}_4 \cdot 2\text{H}_2\text{O}$ single crystal at liquid-nitrogen temperature. Period $t = \tau_0$ in zero field was 2 sec, and H_1 was in a plane perpendicular to the $\langle 010 \rangle$ direction.

and O^{17} . Peaks of the broad direct dipolar absorption¹⁸ by protons were found at 35 and 50 kc/sec for C_{10}H_8 and $\text{CaSO}_4 \cdot 2\text{H}_2\text{O}$, respectively.

While attempting to find the deuterium quadrupole resonance, some interesting effects were found for direct proton dipolar absorption with H_{1B} greater than h_L (in the range from 2 to 10 G for proton solids). As seen in Figs. 15(a) and 16(a), direct dipolar absorption obscures the region of interest for deuterium quadrupole spectra if the irradiation time and intensity of H_{1B} are at the values required for detecting deuterium in natural abundance. An absorption edge at these frequencies is disappointing for detection of deuterium, but not too surprising after calculating¹⁸ the effective relaxation rate caused by the rf field. An interesting and unexpected effect is shown in Figs. 15(b) and 16(b). As H_1 becomes larger than h_L , a narrowing of the direct dipolar absorption is observed. This is possibly explained by a transfer of the A dipolar order into magnetic order along the rotating field H_1 . It may also be related in part to line-narrowing in

¹⁸ A. G. Anderson, *Phys. Rev.* **115**, 863 (1959); **125**, 1517 (1962).

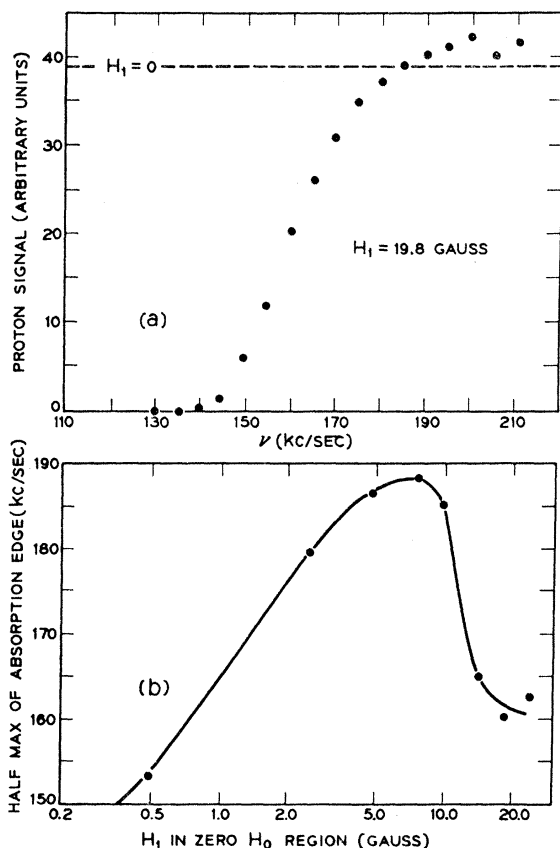


FIG. 16. Zero-field rf absorption for polycrystalline naphthalene, $C_{10}H_8$, at liquid-nitrogen temperature. Period $t = \tau_0$ in zero field was 7 sec.

the rotating frame at the "magic angle," as described by Lee and Goldberg,¹⁹ and to the suppression of proton-proton spin diffusion to paramagnetic impurities because of spin decoupling due to saturation. The latter effect is shown by the proton signals in Figs. 15(a) and 16(a), which increase above the value for zero H_1 . The decoupling of protons from paramagnetic electrons causes an increase in the zero-field spin-lattice relaxation time.

IV. DISCUSSION AND CONCLUSIONS

These experiments show that rare quadrupole moments in concentrations of the order of 10^{-7} of an abundant nuclear species can be detected in zero magnetic field using this double-resonance technique. Identification of the rare nucleus is more difficult than in high-field double-resonance techniques, but the frequency-modulation technique seems to alleviate this difficulty in single crystals and to a lesser extent in powders. The major advantage of the zero-field technique is the ability to observe quadrupole resonances in powders which would be severely broadened in a high magnetic field.

¹⁹ M. Lee and W. I. Goldberg, Phys. Rev. **140**, A1261 (1965).

Resonances observed in NaCl can be compared with theoretical calculations of Dick.²⁰ Only for the K⁺ center are the data understood well enough for comparison. As shown in Table V of Ref. 20, the experimental and theoretical electric field gradients agree within a factor of 2 except for the more distant sites. The Na²³ at the (1, 0, 1) position seems to have a radial electric field gradient principal axis which disagrees with theoretical predictions (see Table III of Ref. 20).

Resonance signal amplitudes that increase with addition of Br⁻ are not clearly identified. The Br⁻ ion in an isolated substitutional site should occupy a centrally symmetric position because of its large ionic radius. Kawamura *et al.*²¹ found evidence for clustering of Br⁻ ions in NaCl, which suggests that a (Br⁻)₂ center may be responsible for the observed resonances. Increased vacancy concentration has also been found for Br⁻ in NaCl. Complex configurations of Br⁻ or Br⁻ with vacancies may be responsible for resonances observed between 200 and 210 kc/sec.

ACKNOWLEDGMENTS

We express our thanks to G. W. Leppelmeier, D. McArthur, D. MacLaughlin, M. Schwab, and R. E. Walstedt for many illuminating discussions, and to J. Koo for constructing experimental apparatus, helpful discussions, and data-taking. One of us (E. L. H.) wishes to thank the Miller Institute for Basic Research at the University of California, Berkeley, for a Miller Professorship, during which a portion of this research was carried out.

APPENDIX: INTERACTION REPRESENTATION FOR NONZERO ASYMMETRY PARAMETER

Consider a single nucleus with spin $S = \frac{3}{2}$ in an asymmetric electric field gradient. The nuclear quadrupole interaction is

$$h_{QB} = K[3S_z^2 - S(S+1) + \frac{1}{2}\eta(S_+^2 + S_-^2)], \quad (A1)$$

where

$$K = e^2qQ/12, \quad (A2)$$

and

$$\eta = (|V_{xx}| - |V_{yy}|) / |V_{zz}| \neq 0. \quad (A3)$$

Hamiltonian terms in S_+^2 and S_-^2 mix the zero η eigenstates $|m_z\rangle = |\pm\frac{3}{2}\rangle$ and $|m_z\rangle = |\pm\frac{1}{2}\rangle$. As a result, all components of a rf field will excite transitions between the two quadrupole energy levels, and the rf-field Hamiltonian at resonance is

$$h_{rfB} = -2\hbar\gamma_B \cos\omega t \sum S_\mu H_{1B\mu}, \quad (A4)$$

where

$$\omega_Q = (e^2qQ/2\hbar)(1 + \frac{1}{3}\eta^2)^{1/2}. \quad (A5)$$

²⁰ B. G. Dick, Phys. Rev. **145**, 609 (1966).

²¹ H. Kawamura, E. Otsuka, and K. Ishiwatari, J. Phys. Soc. Japan **11**, 1064 (1956).

We are interested in finding the energy levels of h_{rfB} and in an interaction representation obtained using the unitary transformation

$$U_Q^\eta = \exp(-i h_{QB} t / \hbar). \quad (\text{A6})$$

h_{QB} is diagonal in the φ representation, where the basis functions are

$$\begin{aligned} \varphi_1 &= \cos\theta \left| +\frac{3}{2} \right\rangle + \sin\theta \left| -\frac{1}{2} \right\rangle, \\ \varphi_2 &= \cos\theta \left| +\frac{1}{2} \right\rangle - \sin\theta \left| -\frac{3}{2} \right\rangle, \\ \varphi_3 &= \cos\theta \left| -\frac{1}{2} \right\rangle - \sin\theta \left| +\frac{3}{2} \right\rangle, \\ \varphi_4 &= \cos\theta \left| -\frac{3}{2} \right\rangle + \sin\theta \left| +\frac{1}{2} \right\rangle, \end{aligned} \quad (\text{A7})$$

and

$$\tan\theta = \eta / (\sqrt{3}[1 + (1 + \frac{1}{3}\eta^2)^{1/2}]). \quad (\text{A8})$$

In the φ representation we obtain

$$h_{rfB} = -\hbar\gamma_B [\exp(i\omega_Q t) + \exp(-i\omega_Q t)] \times \begin{vmatrix} r_{11} & r_{12} & r_{13} & 0 \\ r_{12}^* & r_{22} & r_{23} & -r_{13} \\ r_{13} & r_{23}^* & -r_{22} & r_{12} \\ 0 & -r_{13} & r_{12}^* & -r_{11} \end{vmatrix}, \quad (\text{A9})$$

where

$$\begin{aligned} r_{11} &= \frac{1}{2}(3H_{1Bz}) [\cos^2\theta - \frac{1}{3}(\sin^2\theta)], \\ r_{22} &= \frac{1}{2}(3H_{1Bz}) [\frac{1}{3}(\cos^2\theta) - \sin^2\theta], \\ r_{12} &= H_+ \cos\theta \sin\theta + \frac{1}{2}\sqrt{3}(H_+ \cos^2\theta - H_- \sin^2\theta), \\ r_{23} &= H_- \cos^2\theta - \sqrt{3}H_+ \sin\theta \cos\theta, \\ r_{13} &= -2H_{1Bz} \sin\theta \cos\theta, \end{aligned} \quad (\text{A10})$$

$$\begin{aligned} H_+ &= \frac{1}{2}(H_{1Bz} + iH_{1By}), \\ H_- &= \frac{1}{2}(H_{1Bz} - iH_{1By}). \end{aligned} \quad (\text{A11})$$

Using Pauli spin matrices to express Eq. (A9) and dropping diagonal terms which only cause small frequency shifts, we obtain

$$\begin{aligned} h_{rfB} &= -\hbar\gamma_B [\exp(i\omega_Q t) + \exp(-i\omega_Q t)] \\ &\times \left[\frac{1}{2}r_{12}(\sigma_{a+} + \sigma_{b+}) + \frac{1}{2}r_{23}\sigma_{u-} + \frac{1}{2}r_{12}^*(\sigma_{a-} + \sigma_{b-}) \right. \\ &\quad \left. + \frac{1}{2}r_{23}^*\sigma_{l+} + r_{13}(\sigma_{lz} + \sigma_{uz}) \right]. \end{aligned} \quad (\text{A12})$$

Finally, using transformation Eq. (A6), we find

$$h_{rfB}^* = -\frac{1}{2}(\hbar\gamma_B) \begin{vmatrix} 0 & r_{12} & 2r_{13} & 0 \\ r_{12}^* & 0 & 0 & -2r_{13} \\ 2r_{13} & 0 & 0 & r_{12} \\ 0 & -2r_{13} & r_{12}^* & 0 \end{vmatrix}, \quad (\text{A13})$$

where the prime denotes that terms oscillating at ω_Q and $2\omega_Q$ have been assumed to average to zero. The matrix of Eqs. (A10) is easily diagonalized and we find the eigenvalues

$$\lambda = \pm \frac{1}{2}(\hbar\gamma_B) (4r_{13}^2 + |r_{12}|^2)^{1/2}. \quad (\text{A14})$$

Note that nonzero η does not lift the degeneracy of the energy levels of h_{rfB}^* in the interaction representation. However, the frequency-modulation resonance (see Sec. IIIC) occurs at a frequency which depends on H_{1Bz} , H_{1By} , and H_{1Bz} . Orientation studies could in principle give an experimental value for η if H_{1B} is known from an independent measurement.